CRYSTAL GROWTH & DESIGN

Communication

Cite This: *Cryst. Growth Des.* 2019, 19, 3109−3112

pubs.acs.org/crystal

Linear Zero Thermal Expansion in a Deep-Ultraviolet Transparent Crystal of BPO_4 with Cristobalite-like Structure

Naizheng Wang,[†,⊥] Xingxing Jiang,[*,†,⊥,▽] Maxim S. Molokeev,[‡,¶,#] Gaomin Song,[†,⊥] Shibin Guo,[§] Rongjin Huang,[*,§] Laifeng Li,[§] Yicheng Wu,[∥] and Zheshuai Lin[*,†,⊥,▽]

[†]Technical Institute of Physics and Chemistry, Chinese Academy of Sciences, Beijing 100190, China

[‡]Laboratory of Crystal Physics, Kirensky Institute of Physics, Federal Research Center KSC SB RAS, Krasnoyarsk 660036, Russia

[§]Key Laboratory of Cryogenics, Technical Institute of Physics and Chemistry, Chinese Academy of Sciences, Beijing 100190, China

[∥]Institute of Functional Crystals, Tianjin University of Technology, Tianjin 300384, P. R. China

[⊥]University of the Chinese Academy of Sciences, Beijing 100049, China

[¶]Department of Physics, Far Eastern State Transport University, Khabarovsk 680021, Russia

[#]Siberian Federal University, Krasnoyarsk 660041, Russia

[▽]Center of Materials Science and Optoelectronics Engineering, University of Chinese Academy of Sciences, Beijing 100049, P. R. China

Supporting Information

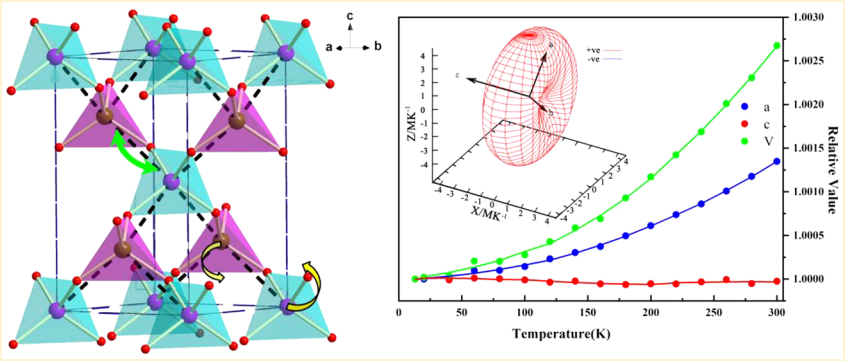

ABSTRACT: We report the discovery of the zero thermal expansion (ZTE) effect in BPO_4, a famous deep-ultraviolet (DUV) optical material with cristobalite-like structure. It is revealed that BPO_4 has a linear ZTE coefficient of −0.16(5) MK^{-1} along the *c*-axis as temperature increases from 13 to 300 K, which originates from the subtle counterbalance between the rotation-induced expansion and contraction effects among BO_4 and PO_4 groups. BPO_4 is a unique DUV cristobalite-like material exhibiting the linear ZTE behavior.

For the optical apparatus operated in complex environments with high temperature-fluctuation, the "heated-expansion and cooled-contraction" effect in optical materials has always been a thorny issue to keep the measurement accurate. Zero thermal expansion (ZTE) materials, in which the size along a specific direction remains constant as temperature varies, could provide an efficient solution to this problem.[1−7] However, optical materials are required to have good optical transmittance, especially in the short wavelength region (e.g., in the deep ultraviolet (DUV) region, λ < 200 nm), since the diffraction limit for an optical device is proportional to the wavelength λ. Recently, increasing number of DUV optical devices have been developed,[8,9] but the discovery of ZTE materials with transparent window down to DUV region still remains challenging.

Cristobalite-like compound family includes a large amount of members, such as the high-temperature phase SiO_2,[10] PON,[11] and $NaAlSiO_4$-serise.[12,13] In these compounds the quasi-rigid tetrahedral anions are connected with each other by sharing the corner atoms to generate the three-dimensional framework structure, while the interstices are empty or occupied by small-radius cations. These materials usually possess excellent optical transmittance in the UV and visible regions, owing to the strong covalent interaction within the tetrahedral anions. Moreover, the rotation of the rigid tetrahedra is the dominant temperature-induced structural modification, which would be possible to achieve the compromise between the thermotropic expansion and contraction and thus give rise to the ZTE behavior along

Received: March 18, 2019
Revised: April 28, 2019
Published: May 6, 2019

DOI: 10.1021/acs.cgd.9b00361
Cryst. Growth Des. 2019, 19, 3109−3112

some specific direction in the cristobalite-like compounds. However, the majority of these materials dissatisfy the volume ZTE criterion proposed by Evans,[14,15] i.e., the opening angles between rigid units should be large enough so that the rotation of these units can be accommodated to keep the cell size unchanged, and therefore have not attracted much attention.

In this work, we discover a unique linear ZTE behavior below room temperature in a cristobalite-like material BPO_4 using the variable-temperature X-ray diffraction (VTXRD). The mechanism for this ZTE behavior is investigated by the first-principles calculations in combination with the variable-temperature Raman spectra (VTRS). We further predict that BPO_4 has ultrastable optical performance in DUV region during the ZTE temperature range.

The crystal structure of BPO_4 is displayed in Figure 1. It crystallizes in a uniaxial $I\bar{4}$ space group with a cristobalite-like

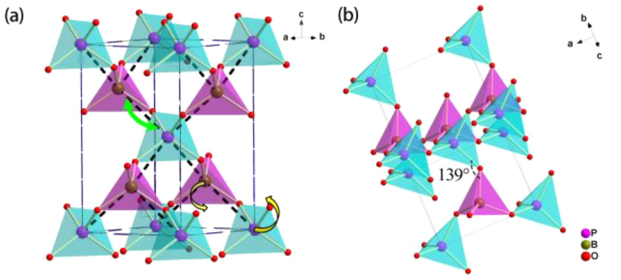

Figure 1. Structure of BPO_4 viewed along (a) (110) and (b) (011) directions. $[BO_4]$and $[PO_4]$ groups are represented by purple and blue tetrahedra, respectively. The B−P distance is highlighted by black dash line. The opening of ∠B−O−P angle is represented by green arrow, and the rotation between the neighboring $[BO_4]$ and $[PO_4]$ tetrahedra is represented by yellow arrows, respectively. Both effects result in the inclination of B−P distance.

structure.[16,17] Each boron (or phosphorus) atom is coordinated with four oxygen atoms to form the $[BO_4]$ (or $[PO_4]$) tetrahedron. By sharing the corner oxygen atoms, $[BO_4]$ and $[PO_4]$ tetrahedra are alternatively connected to one another with the ∠B−O−P angle of 139°, giving rise to the three-dimensional open framework structure. The tetrahedral interstices provide large freedom degree for the rotation of $[BO_4]$ and $[PO_4]$ tetrahedra as temperature varies.

The VTXRD measures on BPO_4 revealed that no new peaks emerge or vanish below room temperature, and all the patterns can be indexed as the $I\bar{4}$ space group (Figure S1). BPO_4 is thermodynamically stable without phase transition, superior to some other cristobalite-type materials.[18−20] The VTXRD cell parameters manifest a strong anisotropy of thermal expansion behavior (Figure 2 and Table S1). As temperature increases from 13 to 300 K, the cell parameter $a(b)$ elongates by 0.13% with the fitted thermal expansion coefficient 4.54(35) MK^{-1} (Figure 2a). In comparison, the cell parameter c almost keeps constant and only changes by less than 0.01% with the fitted thermal expansion coefficient −0.16(5) MK^{-1}, which can be categorized as a typical linear ZTE behavior. The linear ZTE along c-axis is also demonstrated by the observation that the diffraction peaks of (002) plane hardly move as temperature varies (Figure 2b). In fact, BPO_4 has weak linear thermal expansion even under higher temperature: it exhibits a pretty small thermal expansion along the c-axis with the magnitude ∼2/MK between 298 and 1173 K.[21] However, it should be emphasized that the magnitude of the thermal expansion

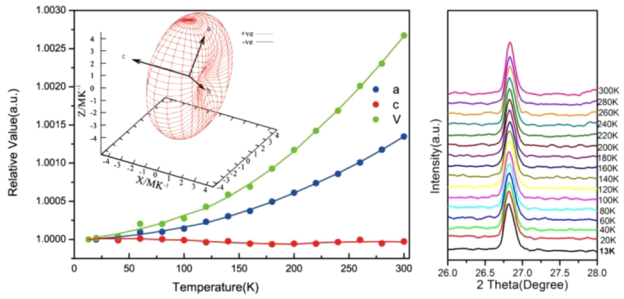

Figure 2. Thermal expansion behavior of BPO_4: (a) evolution of cell parameters with respect to temperature. The insert displays the spatial distribution of thermal expansion coefficient plotted by PASCal software; (b) diffraction peaks for (002) plane in VTXRD patterns under different temperatures. The most intuitive way to investigate the mechanism of the thermal expansion behavior is to trace the variation of bond lengths and angles with respect to the temperature. However, the tiny temperature-induced modification of atomic positions for light boron, phosphorus, and oxygen atoms is difficult to be distinguished using the data collected by laboratory XRD apparatus.[22] Therefore, the temperature-dependent bond lengths and angles were determined by the first-principles stimulations, which have been widely adopted to study the thermal-expansion property of materials.[23,24] The calculated results are listed in Figure 3a and Tables S2 and S3. Clearly, the lengths of B−O and P−O bonds almost keep constant (both elongate by less than 0.01%) as temperature varies from 13 to 300 K, indicating the rigidity of $[BO_4]$ and $[PO_4]$ tetrahedra. Meanwhile, the ∠B−O−P angle increases by 0.18%, more than one order larger than those of B−O and P−O bonds. This confirms that the thermal expansion of BPO_4 is predominantly originated from the rotation between the quasi-rigid $[BO_4]$ and $[PO_4]$ tetrahedra. In fact, the variation of cell parameters is exclusively determined by the B−P distance and its orientation with respect to specific axis. As temperature increases from 13 to 300 K, the opening of the ∠B−O−P angle makes the B−P distance increase from 2.737 to 2.739 Å, which should result in the positive thermal expansion for all the three axes. However, the angle between the B−P distance and c-axis increases from 54.541° to 52.579°, which leads to the thermo-contraction along the c-axis. These expansion and contraction effect counterbalance with each other, giving rise to the linear ZTE behavior along c-axis (as depicted in the inset in Figure 1a).

coefficient along c-axis above room temperature belongs to the range of normal thermal expansion, which cannot be classified to ZTE behavior.

The VTRS were collected to further confirm the mechanism of the linear ZTE behavior of BPO_4. It is because the thermal expansion property is tightly correlated with the anharmonicity of lattice vibrations, which can be characterized from the variation of the phonon frequency with respect to temperature.[5,25−27] As shown in Figure 3b, for all measured temperatures there are seven principal peaks observed in the Raman spectrum (Modes I−VII in Figure 3b and Table S4). Six of them (Modes I and III−VII) are significantly softened as temperature increases, while the frequency of the mode around 459 cm^{-1} (Mode II) exhibits very small shifting with respect to temperature, indicating its key role in the linear ZTE behavior in BPO_4. The first-principle simulations ascribe this mode to the transversal vibration of bridged oxygen atoms, and the vibrational direction is almost parallel to the (a, b) plane and perpendicular to the c-axis (insert in Figure 3b). According to the transverse vibration mechanism,[28,29] the enhanced amplitude of rotation perpendicular to the c-axis between the rigid $[BO_4]$ and $[PO_4]$ tetrahedra would result in a contraction effect of c-axis, which would counterbalance the elongation

DOI: 10.1021/acs.cgd.9b00361
Cryst. Growth Des. 2019, 19, 3109−3112

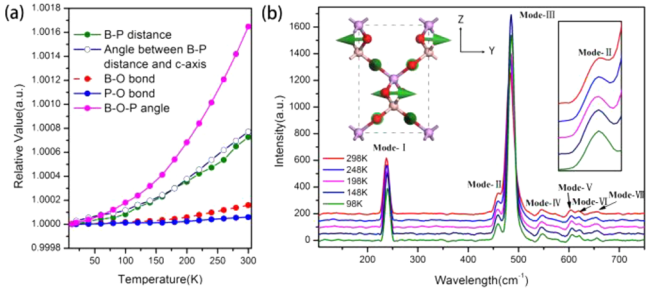

Figure 3. (a) Functions of bond lengths and angles with respect to temperature in BPO_4. (b) Raman spectrum of BPO_4 from 98 to 298 K; the inset in (b) exhibits the atomic vibration projected onto the real space for mode II and magnified spectrum around mode II.

effect originated from the other normal modes and eventually give rise to the ZTE behavior along this direction. Therefore, the linear ZTE behavior of BPO is originated from the anisotropic rotation along the thermal principal axes between the rigid $[BO_4]$ and $[PO_4]$ tetrahedra, consistent with the conclusion deduced from the variation of temperature-dependent bond length and angles.

Remarkably, BPO_4 has excellent optical transmittance in the DUV region with the shortest absorption cutoff of 136 nm among all known cristobalite-type materials.[30−32] The first-principles calculation about the band gap, refractive index, and birefringence demonstrates that the values of these optical properties almost remain constant for the whole ZTE temperatures (Figure 4 and Table S5). This suggests that BPO_4 would be able to generate the ultrastable optical output when exposed to high temperature-fluctuation environments.

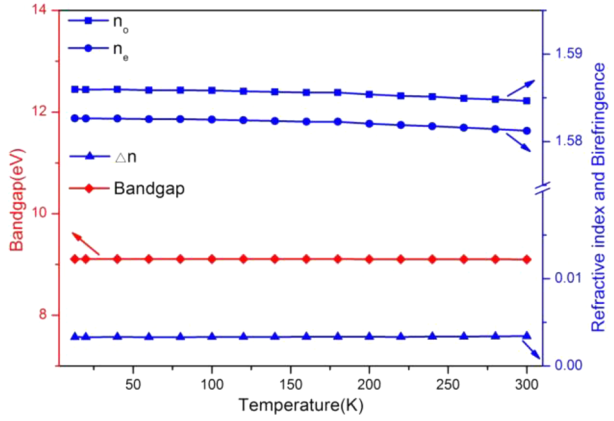

Figure 4. Variation of band gap and refractive index with respect to temperature of BPO_4.

In summary, the thermal expansion behavior below room temperature of BPO_4 with cristobalite-type was studied by variable-temperature X-ray diffraction, and the linear ZTE behavior between 13 and 300 K was discovered. Variable-temperature Raman spectrum and first-principles lattice vibration assignment verified that the linear ZTE behavior is mainly originated from the strong anisotropy of the temperature-induced rotation between the neighboring rigid $[BO_4]$ and $[PO_4]$ tetrahedra. Benefitted from the linear ZTE and excellent optical performance, BPO_4 would find potential application in many highly precise optical facilities operated in high temperature-fluctuating environments, such as space telescope, deep-sea optical sensor, and ultrafine optical grating in cryogenic condition.

■ ASSOCIATED CONTENT

Supporting Information

The Supporting Information is available free of charge on the ACS Publications website at DOI: 10.1021/acs.cgd.9b00361.

VT-XRD, refinement plot for XRD patterns ranging from 13 to 300 K, refined cell parameters of BPO_4 at various temperature, calculated bond length and angles at variable temperature, frequency of the vibrational modes in Raman spectrum from 98 to 298 K, evolution of the frequency of each mode with respect to temperature, calculated band gap, and refractive index and birefringence of BPO_4 from 13 to 300 K (PDF)

■ AUTHOR INFORMATION

Corresponding Authors

*E-mail: zslin@mail.ipc.ac.cn (Z.L.).
*E-mail: xxjiang@mail.ipc.ac.cn (X.J.).
*E-mail: rjhuang@mail.ipc.ac.cn (R.H.).

ORCID

Xingxing Jiang: 0000-0001-6068-8773
Zheshuai Lin: 0000-0002-9829-9893

Notes

The authors declare no competing financial interest.

■ ACKNOWLEDGMENTS

This work was supported by the National Scientific Foundations of China (Grants 51872297, 51702330, 51802321 and 51890864) and Fujian Institute of Innovation (FJCXY18010201) in CAS, and the Youth Innovation Promotion Association in CAS (outstanding member for Z.L. and Grant 2017035 for X.J.).

■ REFERENCES

(1) Sugawara, J.; Kamiya, T.; Mikashima, B. In *Material Technologies and Applications to Optics, Structures, Components, and Sub-Systems III*; Krodel, M., Robichaud, L., Goodman, A., Ed.; SPIE, 2017; Vol. *10372*.

(2) Sawhill, S.; Savrun, E. A Near Zero Coefficient of Thermal Expansion Ceramic: Tantalum Oxyfluoride. *Ceram. Int.* **2012**, *38*, 1981−1989.

(3) Maslov, V. Development of a Technology for Joining Glass-Ceramics Parts with Zero Thermal Expansion. *Opt. Eng.* **2008**, *47*, 023401.

(4) Zhang, Y.; Islam, Z.; Ren, Y.; Parilla, A.; Ahrenkiel, P.; Lee, P.; Mascarenhas, A.; McNevin, J.; Naumov, I.; Fu, H.; Huang, X.; Li, J. Zero Thermal Expansion in a Nanostructured Inorganic-organic Hybrid Crystal. *Phys. Rev. Lett.* **2007**, *99*, 215901.

(5) Jiang, X.; Molokeev, M. S.; Gong, P.; Yang, Y.; Wang, W.; Wang, S.; Wu, S.; Wang, Y.; Huang, R.; Li, L.; Wu, Y.; Xing, X.; Lin, Z. Near-Zero Thermal Expansion and High Ultraviolet Transparency in a Borate Crystal of $Zn_4B_6O_{13}$. *Adv. Mater.* **2016**, *28*, 7936−7940.

(6) Sugawara, J.; Maloney, C. In *Advances in Optical and Mechanical Technologies for Telescopes and Instrumentation II*; Navarro, R.; Burge, H., Ed.; SPIE, 2016; Vol. *9912*.

(7) Chen, J.; Hu, L.; Deng, J.; Xing, X. Negative thermal expansion in functional materials: controllable thermal expansion by chemical modifications. *Chem. Soc. Rev.* **2015**, *44* (11), 3522−67.

(8) Jiang, X.; Joly, N. Y.; Finger, M. A.; Babic, F.; Wong, G. K. L.; Travers, J. C.; Russell, P. S. J. Deep-ultraviolet to mid-infrared supercontinuum generated in solid-core ZBLAN photonic crystal fibre. *Nat. Photonics* **2015**, *9*, 133−139.

DOI: 10.1021/acs.cgd.9b00361
Cryst. Growth Des. 2019, 19, 3109−3112

(9) Tang, L.; Ji, R.; Li, X.; Bai, G.; Liu, C. P.; Hao, J.; Lin, J.; Jiang, H.; Teng, K. S.; Yang, Z.; Lau, S. P. Deep Ultraviolet to Near-Infrared Emission and Photoresponse in Layered N-Doped Graphene Quantum Dots. *ACS Nano* **2014**, *8*, 6312−6320.
(10) Pluth, J. J.; Smith, J. V.; Faber, J. Crystal structure of low cristobalite at 10, 293, and 473 K: Variation of framework geometry with temperature. *J. Appl. Phys.* **1985**, *57*, 1045−1049.
(11) Bykov, M.; Bykova, E.; Dyadkin, V.; Baumann, D.; Schnick, W.; Dubrovinsky, L.; Dubrovinskaia, N. Crystal structures of cristobalite-type and coesite-type PON redetermined on the basis of single-crystal X-ray diffraction data. *Acta Crystallogr. Sect. E-Crystallogr. commun.* **2015**, *71*, 1325−1327.
(12) Withers, R. L.; Lobo, C.; Thompson, J. G.; Schmid, S.; Stranger, R. A modulation wave approach to the structural characterization of three new cristobalite-related sodium magnesiosilicates. *Acta Crystallogr., Sect. B: Struct. Sci.* **1997**, *53*, 203−220.
(13) Husheer, S. L. G.; Thompson, J. G.; Melnitchenko, A. Cristobalite-related phases in the $KAlO_2$-$KAlSiO_4$ system. *J. Solid State Chem.* **1999**, *147*, 624−630.
(14) Evans, J. S. O.; Mary, T. A.; Sleight, A. W. Negative thermal expansion in $Sc_2(WO_4)_3$. *J. Solid State Chem.* **1998**, *137*, 148−160.
(15) Evans, J. S. O.; Mary, T. A.; Sleight, A. W. Negative thermal expansion in a large molybdate and tungstate family. *J. Solid State Chem.* **1997**, *133*, 580−583.
(16) Schulze, G. E. R. The crystal structure of BPO_4 and $BAsO_4$. *Naturwissenschaften* **1933**, *21*, 562.
(17) Achary, S. N.; Jayakumar, O. D.; Tyagi, A. K.; Kulshresththa, S. K. Preparation, phase transition and thermal expansion studies on low-cristobalite type Al1−xGaxPO4 (x = 0.0, 0.20, 0.50, 0.80 and 1.00). *J. Solid State Chem.* **2003**, *176* (1), 37−46.
(18) Haines, J.; Cambon, O.; Hull, S. A neutron diffraction study of quartz-type FePO4: high-temperature behavior and alpha-beta phase transition. *Kristallogr* **2003**, *218*, 193−200.
(19) Worsch, P. M.; Koppelhuber-Bitschnau, B.; Mautner, F. A.; Krempl, P. W.; Wallnofer, W.; Doppler, P.; Gautsch, J. In *European Powder Diffraction, Pts 1 and 2*; Delhez, R.; Mittemeijer, E. J.; Materials Science Forum, 2000; Vol. *321-3*, pp 914−917.
(20) Pagliari, L.; Dapiaggi, M.; Pavese, A.; Francescon, F. A kinetic study of the quartz-cristobalite phase transition. *J. Eur. Ceram. Soc.* **2013**, *33*, 3403−3410.
(21) Achary, S. N.; Tyagi, A. K. Strong anisotropic thermal expansion in cristobalite-type BPO_4. *J. Solid State Chem.* **2004**, *177*, 3918−3926.
(22) Jiang, X.; Luo, S.; Kang, L.; Gong, P.; Yao, W.; Huang, H.; Li, W.; Huang, R.; Wang, W.; Li, Y.; Li, X.; Wu, X.; Lu, P.; Li, L.; Chen, C.; Lin, Z. Isotropic Negative Area Compressibility over Large Pressure Range in Potassium Beryllium Fluoroborate and its Potential Applications in Deep Ultraviolet Region. *Adv. Mater.* **2015**, *27*, 4851−4857.
(23) Li, Y.; Wang, J.; Sun, L.; Wang, J. Mechanisms of ultralow and anisotropic thermal expansion in cordierite $Mg_2Al_4Si_5O_{18}$: Insight from phonon behaviors. *J. Am. Ceram. Soc.* **2018**, *101*, 4708−4718.
(24) Yao, W.; Jiang, X.; Huang, R.; Li, W.; Huang, C.; Lin, Z.; Li, L.; Chen, C. Area negative thermal expansion in a beryllium borate $LiBeBO_3$ with edge sharing tetrahedra. *Chem. Commun.* **2014**, *50*, 13499−13501.
(25) Li, C. W.; Tang, X.; Munoz, J. A.; Keith, J. B.; Tracy, S. J.; Abernathy, D. L.; Fultz, B. Structural Relationship between Negative Thermal Expansion and Quartic Anharmonicity of Cubic ScF_3. *Phys. Rev. Lett.* **2011**, *107*, 195504.
(26) Salke, N. P.; Gupta, M. K.; Rao, R.; Mittal, R.; Deng, J.; Xing, X. Raman and ab initio investigation of negative thermal expansion material TaVO5: Insights into phase stability and anharmonicity. *J. Appl. Phys.* **2015**, *117* (23), 235902.
(27) Cheng, X.; Yuan, J.; Zhu, X.; Yang, K.; Liu, M.; Qi, Z. Origin of negative thermal expansion in Zn2GeO4 revealed by high pressure study. *J. Phys. D: Appl. Phys.* **2018**, *51* (9), 095303.
(28) Evans, J. S. O.; Mary, T. A.; Vogt, T.; Subramanian, M. A.; Sleight, A. W. Negative thermal expansion in ZrW_2O_8 and HfW_2O_8. *Chem. Mater.* **1996**, *8*, 2809−2823.
(29) Chang, D.; Yu, W.; Sun, Q.; Jia, Y. Negative thermal expansion in 2H $CuScO_2$ originating from the cooperation of transverse thermal vibrations of Cu and O atoms. *Phys. Chem. Chem. Phys.* **2017**, *19*, 2067−2072.
(30) Zhang, X.; Wang, L.; Zhang, S.; Wang, G.; Zhao, S.; Zhu, Y.; Wu, Y.; Chen, C. Optical properties of the vacuum-ultraviolet nonlinear optical crystal-BPO_4. *J. Opt. Soc. Am. B* **2011**, *28*, 2236−2239.
(31) Li, Z.; Liu, Q.; Han, S.; Iitaka, T.; Su, H.; Tohyama, T.; Jiang, H.; Dong, Y.; Yang, B.; Zhang, F.; Yang, Z.; Pan, S. Nonlinear electronic polarization and optical response in borophosphate BPO_4. *Phys. Rev. B: Condens. Matter Mater. Phys.* **2016**, *93*, 245125.
(32) Zhao, S.; Zhang, G.; Feng, K.; Lu, J.; Wu, Y. thermophysical and electrical properties of the nonlinear optical crystal BPO_4. *Cryst. Res. Technol.* **2012**, *47*, 391−396.

DOI: 10.1021/acs.cgd.9b00361
Cryst. Growth Des. 2019, 19, 3109−3112